

Electrical Switching of Nematic Plasmonic Nanocolloids for Infrared Solar Gain Control

Souvik Ghosh* and Ivan Smalyukh*

Controlling solar gain is essential to reduce the energy consumption by residential and commercial buildings, which are responsible for $\approx 40\%$ of all energy generated globally. However, the dynamic control of solar gain in the near-infrared that corresponds to $\approx 50\%$ of the overall Sun's energy at the Earth's surface, separately from the visible spectral range has been a challenge, albeit commercial coatings provide passive control while retaining highly visible transmission. To address this problem, in this paper switchable silver colloids (SSCs) are demonstrated, colloidal analogs of the common silver coatings used for solar gain control. When dispersed in a nematic liquid crystal, orientations of such plasmonic silver nanoplates are controlled by ≈ 1 V low-voltage electric fields, allowing for sub-second switching of the near-infrared-based solar gain. Installed and retrofit products made from thin films of such nanoplate dispersions confined between glass and plastic substrates, respectively, exhibit electrically controlled infrared-based solar gain while retaining high visible-range transparency, low haze, and high color rendering index. This study's findings reveal a great potential of soft-matter systems in addressing energy-related problems.

1. Introduction

Plasmonic nanoparticles in colloidal and other dispersions have attracted fundamental research interest^[1] and enabled nanoscale lasers,^[2,3] tweezers,^[4,5] sensors,^[6,7] cancer therapy,^[8,9] and boosted efficiency of solar cells.^[10,11] These dispersed, individualized metallic nanoparticles can produce a variety of different colors, with the best-known example being the stained

glass in windows of old cathedrals, where colors stem from oscillations of free electrons within the gold nanoparticles, vibrating in phase with each other and influencing absorption and scattering of light.^[12] In addition to dispersions in isotropic host media, like glass or water, colloidal dispersions of plasmonic nanoparticles in liquid crystals (LCs) have been demonstrated recently, where localized surface plasmon resonances (LSPR) were partly or fully within the visible spectral range.^[13,14] Recently, plasmonic nanocrystals with tunable properties have been developed for tuning light transmission in both visible and infrared spectral ranges, with anticipated benefits for the energy efficiency of windows and buildings overall.^[15–22] Furthermore, thin silver coatings with high visible transparency are widely used for controlling solar gain and emissivity properties in the infrared in commercial insulating glass units that are nowadays the industry standard.^[23,24] However, solar transmittance through window glazings with permanent coatings cannot be dynamically adjusted according to personal comfort choices with day-to-day variability due to the passive nature of such coatings. In this regard, electrically actuated active light modulation using electrochromic and liquid crystalline materials has enabled next-generation smart glass technology.^[25–27] In recent years, plasmonic transparent conducting oxides have been implemented in electrochromic devices for spectrally selective light absorption, which has significantly reduced the near-infrared solar gain while maintaining good visible light transmittance.^[28–34] On the other hand, using cholesteric LCs both static and dynamic control has been demonstrated by selectively reflecting a band of near-infrared (NIR) wavelengths.^[35–42] Apart from a few limitations from either narrow bandwidth, small but persistent haze, or high switching voltage, the LC-based infrared reflectors can be advantageous in terms of cost compared to electrochromic devices.^[21,43,44] In both of these technologies, optical modulation happens over a similar timescale (approximately minutes) due to their inherent switching mechanisms.

In this work, by orientationally coupling anisotropic nanocolloids with NIR plasmonic resonances to the director in a nematic liquid crystal host medium,^[45,46] we overcome many of the limitations of pre-existing approaches and demonstrate a hybrid metamaterial system that allows for sub-second switching of the NIR solar gain, while maintaining high

S. Ghosh, I. Smalyukh
 Department of Physics
 University of Colorado
 Boulder, CO 80309, USA
 E-mail: souvik.ghosh@colorado.edu; ivan.smalyukh@colorado.edu

I. Smalyukh
 Department of Electrical
 Computer, and Energy Engineering and Materials Science and
 Engineering Program
 University of Colorado
 Boulder, CO 80309, USA

I. Smalyukh
 Renewable and Sustainable Energy Institute
 National Renewable Energy Laboratory
 University of Colorado
 Boulder, CO 80309, USA

 The ORCID identification number(s) for the author(s) of this article can be found under <https://doi.org/10.1002/adom.202201513>.

DOI: 10.1002/adom.202201513

visible transparency, high color rendering index and low haze, which are key to windows-related applications. Since the electric switching relies on a low-voltage ($\approx 1\text{--}10$ V) realignment due to dielectric coupling between the LC director and electric field,^[47] the energy consumption needed for switching is minimal. We discuss how the demonstrated sub-second switching of the near-infrared-based solar gain can be utilized in installed and retrofit glazing products^[26] developed from thin films of such nanoplate dispersions confined between glass and plastic substrates, respectively. We conclude with a discussion of the potential of plasmonic LC nanocolloidal dispersions in enabling the next-generation of glazing products.

2. Results and Discussion

To achieve switchable optical transparency in the near-IR part of the solar spectrum while minimally affecting the visible-range light transmission, careful consideration of experimental parameters and designs is needed. The solution demonstrated here relies on an all-electrical switching of long-range (here shown for inch-scale) self-assembly of 2D plasmonic colloids inside a nematic LC host medium (Figure 1). The switching mechanism works in a reversible manner and applies to planar (where LC molecules align in parallel to a substrate) as well as homeotropic (where LC molecules align perpendicularly to a substrate) cells. We report both vertical alignment (VA) and in-plane switching (IPS) of switchable silver colloids (SSCs), as shown in Figure 1b–d. For the LC host materials with positive dielectric anisotropy, the VA mode can only be used to switch

planar cells whereas the IPS mode enables the switching of both planar and homeotropic cell that requires specialized patterned electrodes on one of the substrates. The key difference between these two configurations is in the way the plasmonic colloids are oriented with respect to the applied field.

The plasmonic colloids used here are commercially available silica-shelled silver nanoplates (AgNPs) of varying diameters (100–200 nm) and fixed thickness (10 nm). The silica shells protect the inner metal nanoplates and retain their plasmonic properties when integrated into composites, allowing for highly stable nanocolloidal dispersions in a wide range of solvents. Due to the shape anisotropy of our nanocolloids, their longitudinal (incident light polarization P parallel to the nanoplates) and transverse (incident light polarization P perpendicular to the nanoplates) LSPR modes differ from each other, with the former designed to be in the near-infrared.^[48] The longitudinal LSPR from the excitation of low energy dipole modes is more pronounced than the transverse LSPR mode peaking at around 400 nm. Three different types of used AgNPs have average lateral dimensions of 125 ± 18 , 159 ± 27 and 181 ± 22 nm, and their longitudinal LSPR spectra peak at ≈ 825 , ≈ 950 and ≈ 1020 nm, respectively (Figure S1, Supporting Information). The broadband near-infrared extinction spectra are desirable for the envisaged solar gain control and are primarily due to high polydispersity in the shapes and lateral dimensions of the nanoplates. For AgNPs having an LSPR peak at 1020 nm, the extinction peak nearly overlaps with the infrared-A range (IR-A, 780–1400 nm, defined by the Commission Internationale de l'Eclairage [CIE])^[49] of the solar spectrum while having minimal absorption at the visible wavelengths, as shown in Figure 2a.

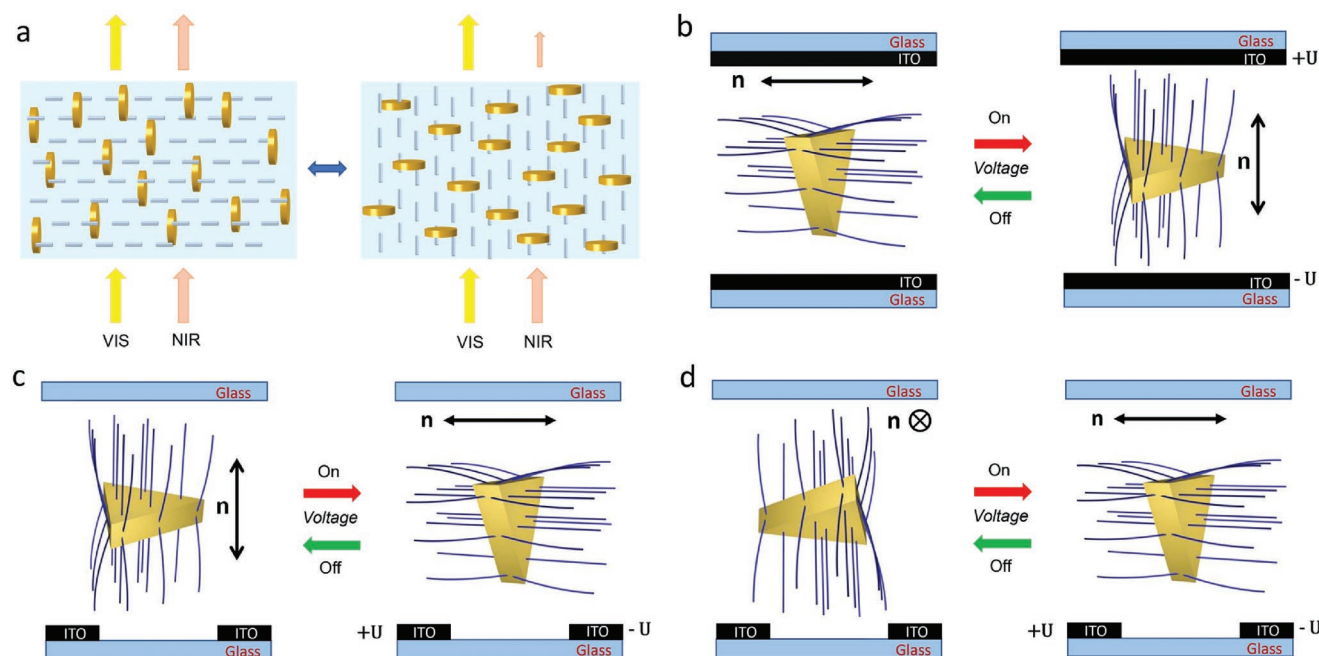


Figure 1. Schematic illustrations of physical mechanisms behind near-IR transmission switching. a) Reversible switching of near-IR selective transparency using plasmonic silver nanoplates homogeneously dispersed in an anisotropic LC fluid. b) Schematic of electric switching of Ag nanoplate dispersions inside a planar LC cell with voltage applied across the cell using electrodes on the opposite confining surfaces. c,d) Schematic of electric switching of Ag nanoplate dispersions inside c) a homeotropic and d) a planar cell, which utilizes in-plane electric fields generated with patterned electrodes located on the bottom substrate. Blue lines indicate LC director orientation around the Ag nanoplate. Figure not to scale.

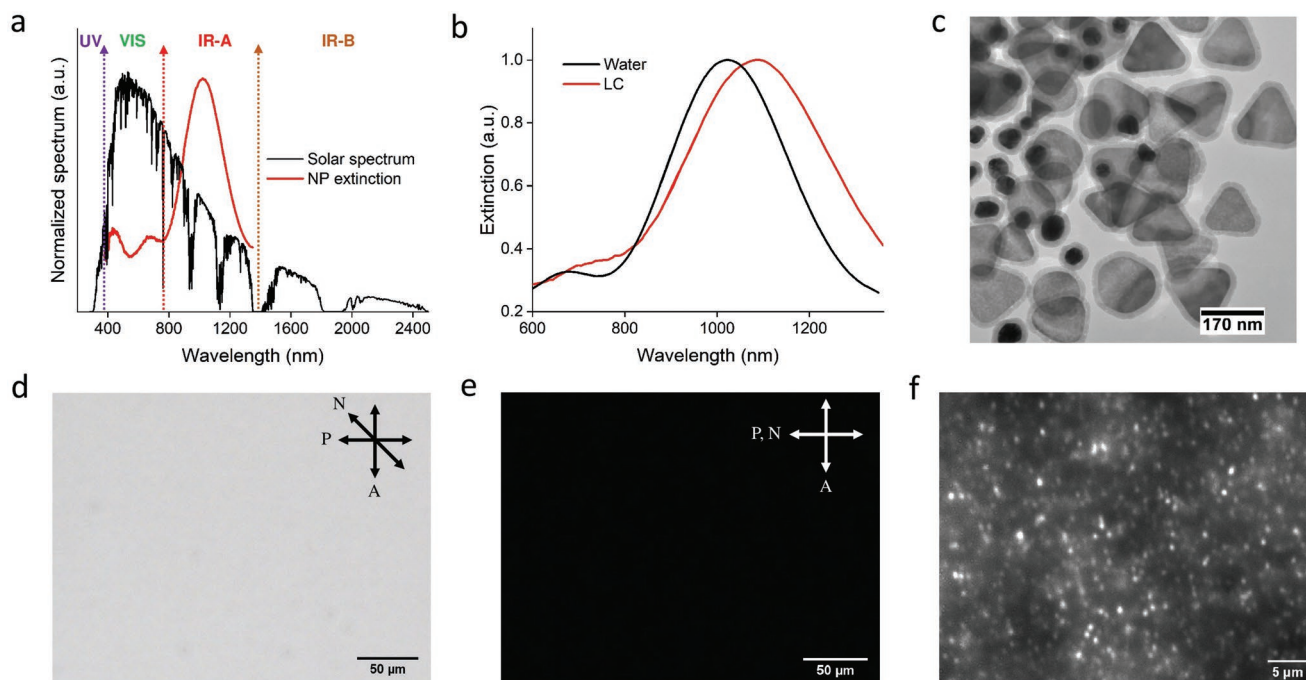


Figure 2. Dispersion of plasmonic nanoplates in 5CB liquid crystal. a) Solar irradiation intensity at the Earth's surface and absorption of the plasmonic nanoplates dispersed in water versus wavelength. The graph shows maximal plasmonic absorption in the IR-A range of the solar spectrum while absorbing minimally at the visible-range wavelengths. b) Extinction spectra of the AgNPs dispersed in water and 5CB. c) Transmission electron microscopy image of the nanoplates clearly showing the thin silica shell at the periphery of the AgNPs obtained from nanoComposix Inc. d,e) Polarizing optical micrographs of the monodomain LC-nanoplate composite with the director N at d) 45° and e) 0° to P. f) Dark-field micrograph of the composite showing scattering from individual AgNPs dispersed in the 5CB host medium.

The formulation of mixtures of nanoplate dispersions can allow for further broadening and optimizing the infrared spectral characteristics depending on the needs, like climate zones, etc. The LSPR peak slightly redshifts and the extinction spectra also get somewhat broadened (Figure 2b) when the AgNPs are dispersed in a nematic LC host instead of water. The reason is attributed to an increased effective refractive index as well as to its anisotropy and the inhomogeneity of its distribution around the AgNPs in a nematic host medium. Note that, compared to other plasmonic metals, silver is preferred due to its excellent qualities in terms of plasmonic ability (highest quality factor among all plasmonic materials) and reasonable material cost.^[50] As reported in the literature, the Ag nanoplates used in our work are highly reflective in nature. In general, the relative strengths of absorption and scattering/reflection for a plasmonic nanoparticle depend on the particle's size, shape, and material properties. For Ag nanodisks with a mean diameter larger than 100 nm, scattering strongly dominates over absorption.^[51,52] Specifically, for Ag nanoplates (similar dimensions as ours), the absorption to reflection ratio can be as high as 1:3.^[53,54] Using such 10 nm-thick Ag nanoplates, Fujifilm Inc. demonstrated a transparent near-infrared reflector by randomly dispersing the nanoparticles as a coating on a plastic substrate.^[55] As the nanoparticle density was increased, the scattering for near-infrared wavelengths increased monotonically, while the absorption saturates. We expect similar reflection/absorption properties in our system as well.

To disperse the silica-shelled nanocolloids (Figure 2c) in the LC, the silica surfaces were treated with surfactants like

dimethyloctadecyl[3-(trimethoxysilyl)propyl]ammonium chloride (DMOAP), known to produce perpendicular surface boundary conditions for anisotropic host LC molecules (see Experimental Section). When dispersed in nematic LCs, such as 4-cyano-4'-pentylbiphenyl (5CB), the AgNPs due to finite-strength boundary conditions on their surfaces align perpendicular to the local nematic director N describing the average orientation of rod-like organic molecules. The monocrystal-like orientational order of LC-AgNP dispersion inside a closed planar cell is observed with polarizing optical microscopy (Figure 2d,e) by rotating the sample between two crossed polarizers. Furthermore, micrographs shown in Figure 2d,e confirm that the AgNPs do not significantly perturb the uniform alignment of the LC host. Additionally, dark-field imaging (Figure 2f) reveals that the AgNPs are dispersed individually and undergo Brownian motion as individual nanoparticles at high mass concentrations greater than 1 mg mL⁻¹. This behavior is possible thanks to their small thickness and pre-designed boundary conditions and geometry, which induce only weak director distortions around the nanoplates. Further, the electrostatic repulsions enabled by colloidal surface charging, which stem from charged DMOAP molecules on the nanoplates' surfaces, counterbalance the weak elastic attractions among the particles associated with the director distortions.

Owing to the long-range orientational order of the SSCs, optical transmittance through the composite depends on the alignment of the AgNPs. A nematic host LC allows us to dynamically tune its orientation in a reversible fashion using low electrical voltage. The dispersed colloids then follow the change in

nematic director orientation as the nanoparticle's alignment is mechanically coupled to that of the LC director N . To utilize this facile response to the applied electrical stimuli, the dispersions of AgNPs in 5CB are infiltrated into planar cells made from glass plates coated with transparent and conducting indium tin oxide (ITO) on their inner surfaces. Within the LC host, the AgNPs align perpendicular to the local average molecular orientation, having their surface normals orientationally ordered along the nematic director N . Therefore, when we illuminate the cell with light polarized along the nematic director N , the transverse LSPR mode is excited and the transmitted NIR light is affected the least as a result. Subsequently, with an application of a finite voltage at frequencies of 1 kHz in between the ITO surfaces, the AgNPs reorient themselves with the surface normal aligned vertically, as shown in Figure 1b. Consequently, with an increase in voltage longitudinal LSPR mode dominates reducing the NIR transmittance, as shown in Figure 3a. At the resonance wavelength in the near-IR range, the light transmission drops $\approx 35\%$ from the initial state, leading to a 20% overall change in NIR transmittance when the cell is fully switched. This optical modulation remains consistent in over at least 500 switching cycles (Figure 3a,b). The dynamic switching over a few cycles has been shown in Figure S2, Supporting Information, using a square wave electric signal. Note that, we did not perform the cycling test until failure. The composite remains

transparent before and after switching as the overall visible-range transmittance does not differ much between the two orientational states of the AgNPs (see Figure 3b). Also important is diffused transmission as it can cause a hazy appearance. Maintaining low haze is crucial for window-related applications. From the spectral data shown in Figure 3b, we measure less than a 2% change in the haze of the composite cell compared to the pristine LC cell, owing to the particle dimensions smaller than the visible wavelengths. In our composite cell light scattered/reflected by the Ag nanoplates is evanescent and is located around the particles. Additionally, as these particles are very thin and are smaller in size compared to the visible wavelengths, the light scattering is Rayleigh type which does not contribute significantly to a hazy appearance. Thus, when viewed in the far field region, the composite appears uniformly transparent. In the two extreme orientations at 0 and 10 V respectively, the visible light scattering from the transparent composite is very weak and does not change significantly at different orientations depending on the applied voltage. This is consistent with literature findings for similar Ag nanoplates coated on a substrate at a fixed orientation, which also reported a low haze.^[53,54] Despite the highly concentrated dispersion of AgNPs, the acceptable low haze value that we measure confirms the fact that the colloids are uniformly dispersed throughout the glass cell. The near-IR light transmission through the cell

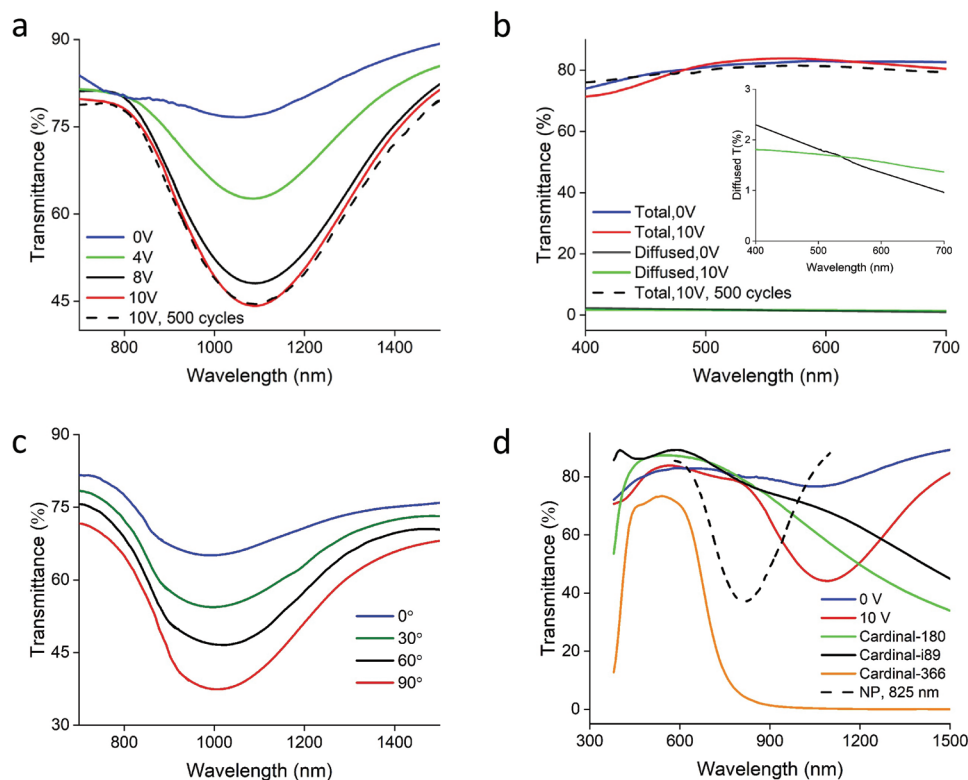


Figure 3. Optical response of the SSCs in different spectral ranges. a) Transmittance versus wavelength plot for the composite in the IR-A range at different applied voltages. The transmission properties remain unchanged after at least 500 cycles. b) Total transmittance of the composite in the visible range and the change of diffused transmittance of pure 5CB after the addition of AgNPs, with and without voltage. A zoomed-in view of diffused transmittance plot is shown in the inset. c) Transmittance versus wavelength plot of the composite in the IR-A spectral range at different linear polarization angles of incident light. d) Transmittance spectra of the composite without (0 V) and with applied voltage (10 V) as compared to three different commercially available coated glass products (Cardinal glass products, with the commercial names shown in the legend). The dashed curve shows the data for a fully switched cell with a different set of nanoplates having an LSPR peak at 825 nm.

can also be tuned by rotating the polarization of incident illumination with respect to nematic director N as the unidirectional self-alignment of the AgNPs in the nematic LC induces polarization-dependent LSPR properties of the entire inch-scale composite, as shown in Figure 3c. These results are consistent up to the nematic to isotropic transition temperature of the composite $T_{NI} = 33.8$ °C which is slightly lower than the T_{NI} of pure 5CB. Next, we compare (Figure 3d) the transmission spectra of our LC-AgNP composite before and after switching with commercially available coated glasses designed for similar purposes, albeit with only passive control of the solar gain. A comparison between the commercial glasses and the glass cells with our composite at different voltages is shown in Table 1 with respect to the target parameters of near-IR

solar gain coefficient $SHGC_{NIR} = \frac{\int_{780}^{1400} T(\lambda)E(\lambda)d\lambda}{\int_{780}^{1400} E(\lambda)d\lambda}$ and visible

light transmittance $VLT = \frac{\int_{380}^{780} T(\lambda)V(\lambda)E(\lambda)d\lambda}{\int_{380}^{780} V(\lambda)E(\lambda)d\lambda}$, where $T(\lambda)$

is wavelength-dependent transmission, $E(\lambda)$ is solar irradiance spectra on earth and $V(\lambda)$ is the spectral response of the human eye. Our active composite cell not only provides visible transparency comparable to or better than the passive coated glasses but also offers dynamically tunable near-IR solar gain. Interest-

Table 1. Comparison of the visible light transmittance and solar heat gain coefficient for our AgNP-LC composite cells at different voltages, as well as the comparison to the performance of the commercially available passive glass products. *Data from Cardinal Glass Inc.

| | VLT | SHGC _{NIR} |
|--------|-------|---------------------|
| C-180* | 0.8 | 0.65 |
| C-i89* | 0.876 | 0.71 |
| 0 V | 0.831 | 0.8 |
| 4 V | 0.827 | 0.71 |
| 8 V | 0.825 | 0.63 |
| 10 V | 0.823 | 0.6 |

ingly, the “passive” or “off” state of the SSCs can be designed for appropriate climate conditions such as to promote energy-saving benefits and reduce the frequency of needed switching. As shown in Figure 3b, the VA mode exhibits high near-IR transmission in the “off” state, and therefore it would be preferred for regions having long winters. Alternately, in hot climates with short winters, where controlling high solar gain is important, the operation could utilize the default “off” state in IPS configuration, as shown in Figure 1c.

The plasmonic-LC composite responds to an applied electric field in a similar way as the pure LC. Figure 4a,b demonstrates the characterization of the electric switching response time of

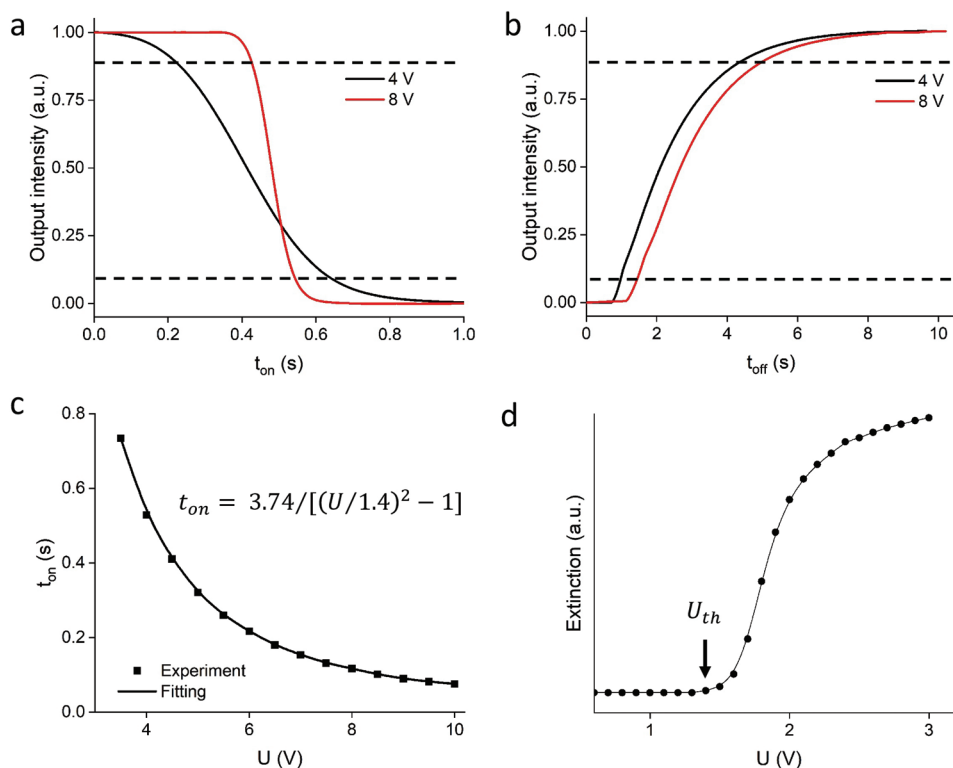


Figure 4. Electric switching of the SSCs. a) Typical dependencies of transmitted intensity used to determine the voltage-on switching time t_{on} of the composite at two different voltages when an electric field is applied vertically to a 40 μm thick planar cell. b) Typical dependencies of intensity used to determine the voltage-off switching time t_{off} of the composite at two different voltages when the electric field is turned off. c) Switching time t_{on} versus the amplitude of applied voltage U . The fitting expression is shown next to the fitting curve. The output intensity change between the two dashed lines (0.1 and 0.9 in (a) and (b)) was used to determine the switching times. d) Extinction of the composite versus applied voltage plot. The black arrow marks the threshold voltage U_{th} .

the SSCs inside a planar cell for two different voltages, 4 and 8 V, applied orthogonally to substrates. Similar to the case of a pristine LC, with applying voltage above a threshold voltage, the optical output of the composite varies nonmonotonously over a sub-second timescale. With an increasing amplitude of the applied voltage, the director and nanoplate orientation switching happens faster, thereby reducing the response time t_{on} . Subsequently, when the electric field is taken away, the relaxation switching happens over a significantly longer duration, and the turning-off response time t_{off} is independent of the applied voltage (see Figure 4b). The response times are measured based on the transmitted intensity changes between 10% and 90%, as marked by dotted lines in Figure 4a,b. For a 40 μm thick cell, at a typical applied voltage of 8 V, t_{on} and t_{off} are found to be 0.117 s and 3.74 s, respectively. Likewise, for an IPS cell with cell gap and applied voltage as in the previous example, we observe similar response times (see Figure S3, Supporting Information). However, the threshold voltage U_{th} required for switching is different in these two scenarios. In the case of the VA mode, U_{th} characterized based on the extinction versus applied voltage plot (Figure 4d) is found to be 1.4 V while in the IPS mode the threshold voltage is nearly 2 V as obtained from the data shown in Figure S3b, Supporting Information. Next, we show in Figure 4c that t_{on} is reducing with the increase of applied voltage, with the dependence fitted with the theoretical formula for pristine LCs, $t_{\text{on}} = t_{\text{off}} / [(U/U_{\text{th}})^2 - 1]$, where U_{th} is the threshold voltage required for switching. From this fitting, the threshold voltage is estimated to be 1.42 V which closely matches the experimental value obtained from the extinction versus applied voltage plot. This value of U_{th} for the LC-nanocolloidal plasmonic composite is marginally higher than that for the pristine 5CB because concentrated dispersions

of metal nanoparticles can slightly influence the elastic and dielectric LC properties as compared to pristine materials. Similar nanoinclusions-related modification can happen to the viscoelastic properties of the host LC as well, albeit they are minor, and probing them in detail is outside of this work's scope. Indeed, the rotational viscosity γ_1 of our LC-AgNP composite is found to be 147 mPa S from the theoretical formula $t_{\text{off}} = \gamma_1 d^2 / K_{11} \pi^2$ where d is cell gap and K_{11} is splay elastic constant, which is also increased a bit compared to $\gamma_1 \approx 81$ mPa S of pristine 5CB, consistent with findings of previous studies.^[15]

An important factor for window applications is related to the aesthetically acceptable neutral colors. To quantify color neutrality, we calculated color perception indices using the CIE 1931 xy color space, designed to represent the human visual color perception. As shown in Figure 5a, the AgNP-LC composite cell has chromaticity coordinates of (0.3384, 0.3384) as obtained from the transmitted light through the cell which changes only slightly to (0.3374, 0.3413) with an application of voltage. In both voltage-on and voltage-off cases, the chromaticity coordinates are situated in the low colorfulness region of the chromaticity diagram, representing excellent color-neutrality. Moreover, the composite cell achieves a color-rendering index of CRI = 87 (0 V) and 89 (10 V). This high CRI value indicates that illumination through the cell accurately renders the true color of an object under observation. Under natural sunlight, the photographs of an IPS cell switched from homeotropic to planar state appear to be color neutral, as shown in Figure 5b,c. The CU logo is clearly visible without any noticeable change in color in both these pictures. A uniform tinting effect is present due to the slightly reduced visible transmission, however, that does not significantly depend on the SSCs orientation within the glass cell.

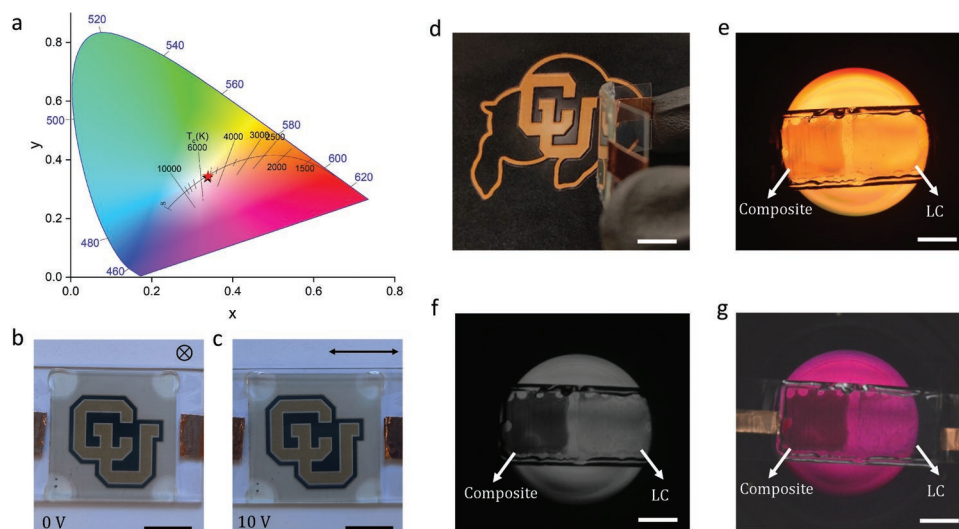


Figure 5. Optical performance of the composite. a) Perceived color and color temperature of the cell with the composite in between two ITO-coated glass substrates represented in the CIE1931 chromaticity diagram. The black and red stars represent the data for 0 and 10 V applied to the cell, respectively. b,c) Photographs of the typical IPS cell with a thickness of 40 μm under natural daylight with b) 0 and c) 10 V applied electric voltage. d) Photograph of the AgNP-LC composite inside a flexible cell formed by the ITO-coated PET substrates. e) Photograph of the plastic LC cell under visible light illumination. f) Infrared photograph of the cell with the backlit illumination. g) Full-spectrum photograph of the cell with infrared backlit illumination. As shown in the photos (d)–(g), the cell is divided into two parts using epoxy where the left part contains AgNP-LC composite, and the right part contains just the LC. Photographs with backlit illumination show a strong contrast between the two parts in near-IR which, however, is weak under visible light, demonstrating selective near-IR light-blocking properties of the AgNP-LC composite. All scale bars are 1 cm.

Beyond glass, we have tested our composite when confined with the help of flexible substrates as well. This configuration is an “applied product” embodiment of our technology and is beneficial for a number of applications where the composite-based products can be adapted to specific surface requirements, such as retrofitting an already installed window, thereby promoting the versatility of its use. To prepare a flexible LC panel, as shown in Figure 5d, AgNP-LC dispersion is sandwiched between two optically clear ITO-coated polyethylene terephthalate (PET) sheets with homeotropic surface anchoring (see Experimental Section) and separated by a 40 μm cell gap. The flexible cell is divided into two parts containing the composite and pure 5CB within the respective compartments with the LC director aligning perpendicular to the substrates. The surface normal of the nanoplates having homeotropic anchoring orient themselves along the LC director N without applying any voltage. As a result, longitudinal LSPR mode dominates under normal light incidence reducing the overall NIR transmittance. For a direct visual comparison among the two parts for the visible and near-IR wavelengths, the flexible cell is illuminated by a tungsten-halogen lamp that generates a continuous spectrum of light from the central ultraviolet through the visible and into the infrared wavelength regions. As can be seen from Figure 5e, under visible light illumination the two parts appear nearly similar, exhibiting low contrast among them. However, in the near-IR the contrast between the two sides is noticeably increased, further confirming the energy-saving potential of the LC-nanocolloidal composite (see Figure 5f,g). A simple calculation has shown that $\approx 9\%$ of a standard building’s energy usage can be saved by using this smart switchable composite (see Supporting Information). Also important is the power consumption of the LC-cell for switching and maintaining its on-state. The LC composite material is overall dielectric in nature even after doping with nanoparticles.^[56] Therefore, the device acts as a capacitor overall which is equivalent to a one-pixel LCD from the power consumption standpoint. From an order of magnitude approximation, the total energy consumption to run and maintain the device is only 20 mW m^{-2} , which is significantly lower than the energy required by the most efficient electrochromic^[33] and cholesteric-LC^[38]-based NIR-selective smart glasses reported to date (see Supporting Information).

There are several interesting opportunities to enhance the current capabilities of SSCs: i) due to the low voltage switching, our device can be powered by a battery or a solar cell without requiring additional electrical wiring in the building; ii) future designs can incorporate different plasmonic colloids with pre-designed LSPR properties^[57–59] at desired wavelengths of operation, as well as a co-dispersed combination of them may increase the bandwidth of modulation; iii) one may use higher concentrations of plasmonic colloids to enhance the tinting effect and, thus, increase the solar gain control, which may eventually allow for blocking near-IR transmissivity completely; iv) SSCs can be further designed to add privacy control functionality, for example, by co-dispersing the silver nanoplates with other nanoparticles or dyes while producing aesthetically appealing colors;^[60] v) integration with intensity or temperature sensors with the LC module can allow for automating the solar gain control, depending on the surrounding environment

and personal comfort choices; and vi) it may be possible to harvest a significant portion of the scattered solar energy from the SSCs for energy generation. Part of the scattered light that gets trapped inside the LC panel by total internal reflection can subsequently be guided toward the photovoltaic cells placed along the edges.^[61] A similar mechanism may be feasible also for the absorbed solar energy using thermophotovoltaics.^[62]

3. Conclusion

The experimental designs presented in this work demonstrate the visibly transparent near-IR-selective optical modulation at sub-second switching speeds with excellent color neutrality. Our work presents an approach potentially capable of overcoming the limitations of the dynamic windows’ technologies for controlling solar gain in the near-infrared while also allowing for unimpeded light transmission in the visible spectral range as well as helping to block the ultraviolet portion of the solar radiation. Apart from this, the composite system is extremely power efficient requiring only 20 mW m^{-2} for switching and maintaining the “on” state, thereby providing $\approx 9\%$ energy savings. With their development prompted by the needs of the display industry, there is a large variety of available chemical compounds and their mixtures that exhibit the nematic phase within a broad thermal range, which will aid in the deployment of such dynamic windows in different climate zones. Furthermore, by integrating such window products with highly thermally insulating materials, such as aerogels,^[63] one could additionally boost the energy-saving capability of new window designs by additionally eliminating the energy loss through thermal conduction.

To conclude, we have demonstrated colloidal nanoplate dispersions in LC hosts that are capable of tuning solar gain due to the near-infrared component of the solar spectrum. The envisaged products, including windows and skylights, can take the forms of glass cells with thin films of plasmonic nanocolloidal dispersions in LCs sandwiched in-between and controlled by low voltages applied to confining substrates, as well as similar designs that involve plastic substrates, as needed for products designed for retrofitting the pre-existing windows.

4. Experimental Section

Dispersion of Colloidal Nanoparticles: The authors used silica-shelled silver nanoplates purchased from nanoComposix (San Diego) at 1 mg mL^{-1} mass concentration in an aqueous 10 mM sodium bicarbonate buffer. The particles were at first washed once with deionized water and twice with ethanol. In the next step, the nanoparticles were surface-functionalized by DMOAP (purchased from Acros Organics) through a two-step method that proceeded as follows. First, 0.1 mL of nanoparticle solution was mixed with 0.9 mL ethanol. After that, $10 \mu\text{L}$ of the ethanol solution of (3-mercaptopropyl)trimethoxysilane (MPTMS) (10% in volume) was added to the solution. The mixture was sonicated for 20 min , centrifuged at 7000 rpm for 10 min , and then redispersed in 1 mL of methanol. Then, a few drops of the DMOAP solution at $60 \text{ wt}\%$ in methanol was added to achieve a 1% mass concentration. The mixture was sonicated for another 20 min , washed and centrifuged, and then washed again three times at 7000 rpm for 10 min in methanol. Finally, the nanoparticles were redispersed in methanol to achieve a 1 mg mL^{-1}

mass concentration. This as-prepared colloidal dispersion was stored in a refrigerator and used in the desired amount for experiments. In a typical experiment, 30 μL of the nanoparticle dispersion was mixed with 20 μL of pure 4-cyano-4'-pentylbiphenyl (5CB, from Chengzhi Yonghua Display Materials Co. Ltd.) at room temperature. The mixture was kept inside an oven at 80 $^{\circ}\text{C}$ until all the methanol was fully evaporated. The resultant isotropic mixture was then sonicated in a water bath at 80 $^{\circ}\text{C}$ for 4 min and then quenched to the nematic phase while having been agitated mechanically. This process was then followed by centrifugation at 2000 rpm for 3 min to separate out the aggregates formed during the LC phase transition, resulting in a uniform colloidal dispersion.

Sample Fabrication: The LC cells were prepared using glass substrates coated with transparent ITO electrodes on the inner surfaces to enable the application of electric fields. The authors used two types of ITO electrodes to design their experiments. The uniformly coated ITO thin films covering the entire glass surfaces of confining substrates were used to apply electric fields perpendicular to the glass substrates (for vertical alignment) and the micropatterned ITO coatings were used to apply electric fields tangential to the glass surface (for in-plane switching). To prepare, LC cells with planar surface anchoring the ITO-coated surfaces were spin-coated with 1 wt% aqueous polyvinyl alcohol (PVA, from Sigma Aldrich) and baked at 100 $^{\circ}\text{C}$ for 1 h. The PVA-coated surfaces were then rubbed unidirectionally with a soft velvet cloth to define the direction for the director N and then glued together with UV-curable NOA-65 glue (Norland Products, Inc.) containing spacers (such as the 40 μm silica spheres) to define the desired cell gap. For the homeotropic LC cells, the ITO-patterned surfaces of the glass plates were spin-coated with a polymer SE5661 and baked at 185 $^{\circ}\text{C}$ for 1 h. Homeotropic anchoring on the ITO-coated flexible PET substrates (from Thorlabs) was done by vapor phase deposition of 1H, 1H, 2H, 2H-perfluorooctyltriethoxysilane under vacuum condition.^[64]

Electro-Optical characterization: For optical microscopy observations, the authors used an Olympus BX-51 upright polarizing optical microscope with the 10 \times air objective having a numerical aperture of 0.3 and a charge-coupled device (CCD) camera purchased from Pointgrey. For dark-field imaging, the sample was illuminated with an oil-immersion dark-field condenser (numerical aperture of 1.2), and the highly scattered light was collected with a 100 \times , variable numerical aperture (0.6–1.3) oil immersion objective and imaged with another monochrome CCD camera (Spot Pursuit, Diagnostic Inc.). The extinction and transmission spectra were studied using two separate spectrometers dedicated to visible (Silver Nova, from Stellernet Inc.) and near-IR wavelengths (Dwarf Star, from Stellernet Inc.) mounted on the microscope. The broad-spectrum light was collected using Y-type optical fiber with a 600 μm core diameter. The collected light was split into two parts and coupled to the respective spectrometers. The electric switching of the composite was characterized using a data acquisition system (USB-6259, from National Instruments Co.) controlled by a homemade software written in LabVIEW (from National Instruments Co.), and a Si-amplified photodetector (PDA100A2, from Thorlabs Inc.). For the switching time measurements of the composites of 5CB and silver nanoplates, visible light filters were used to block visible light spectra and allow only the near-IR light that includes the longitudinal LSPR peak of the AgNPs. The photographs of the flexible cells were taken with a D3200 camera (from Nikon). The IR photographs were taken using a 850 nm long-pass filter.

Supporting Information

Supporting Information is available from the Wiley Online Library or from the author.

Acknowledgements

The authors acknowledge the discussions and technical assistance of Ye Yuan. S.G. thanks B. Senyuk, T. Lee, J. B. Ten Hove, E. Abraham for helpful

discussions, and P. B. De Melo for the help in taking the photographs. I.S. acknowledges funding from the US National Science Foundation's Division of Innovation and Partnership grant IIP-2044762. I.S. and S.G. thank the US Department of Energy, Office of Basic Energy Sciences, Division of Materials Sciences and Engineering, under contract DE-SC0019293 with the University of Colorado at Boulder for supporting the work.

Conflict of Interest

The authors declare no conflict of interest.

Data Availability Statement

The data that support the findings of this study are available from the corresponding author upon reasonable request.

Keywords

electro-optic switching, liquid crystals, plasmonic colloids, self-assembly, solar gain, transparent smart windows

Received: July 1, 2022

Published online:

- [1] S. Enoch, N. Bonod, *Plasmonics*, (Eds: S. Enoch, N. Bonod), Vol. 167, Springer Berlin Heidelberg, Berlin, Heidelberg **2012**.
- [2] S. I. Azzam, A. V. Kildishev, R. M. Ma, C. Z. Ning, R. Oulton, V. M. Shalaev, M. I. Stockman, J. L. Xu, X. Zhang, *Light: Sci. Appl.* **2020**, 9, 90.
- [3] M. A. Noginov, G. Zhu, A. M. Belgrave, R. Bakker, V. M. Shalaev, E. E. Narimanov, S. Stout, E. Herz, T. Suteewong, U. Wiesner, *Nature* **2009**, 460, 1110.
- [4] S. Ghosh, A. Ghosh, *Nat. Commun.* **2019**, 10, 4191.
- [5] S. Ghosh, A. Ghosh, *Langmuir* **2020**, 36, 5691.
- [6] J. N. Anker, W. P. Hall, O. Lyandres, N. C. Shah, J. Zhao, R. P. Van Duyne, *Nat. Mater.* **2008**, 7, 442.
- [7] A. J. Haes, R. P. Van Duyne, *J. Am. Chem. Soc.* **2002**, 124, 10596.
- [8] M. Kim, J. H. Lee, J. M. Nam, *Adv. Sci.* **2019**, 6, 1900471.
- [9] P. K. Jain, X. Huang, I. H. El-Sayed, M. A. El-Sayed, *Acc. Chem. Res.* **2008**, 41, 1578.
- [10] H. A. Atwater, A. Polman, *Nat. Mater.* **2010**, 9, 205.
- [11] Y. H. Jang, Y. J. Jang, S. Kim, L. N. Quan, K. Chung, D. H. Kim, *Chem. Rev.* **2016**, 116, 14982.
- [12] S. A. Maier, *Plasmonics: Fundamentals and Applications*, Vol. 677, Springer US, New York, NY **2007**.
- [13] Q. Liu, Y. Yuan, I. I. Smalyukh, *Nano Lett.* **2014**, 14, 4071.
- [14] Y. Zhang, Q. Liu, H. Mundoor, Y. Yuan, I. I. Smalyukh, *ACS Nano* **2015**, 9, 3097.
- [15] H. Takeda, K. Adachi, *J. Am. Ceram. Soc.* **2007**, 90, 4059.
- [16] K. Manthiram, A. P. Alivisatos, *J. Am. Chem. Soc.* **2012**, 134, 3995.
- [17] A. Lordés, Y. Wang, A. Fernandez-Martinez, P. Xiao, T. Lee, A. Poulain, O. Zandi, C. A. S. Cabezas, G. Henkelman, D. J. Milliron, *Nat. Mater.* **2016**, 15, 1267.
- [18] R. Buonsanti, A. Llordés, S. Aloni, B. A. Helms, D. J. Milliron, *Nano Lett.* **2011**, 11, 4706.
- [19] A. Llordés, G. Garcia, J. Gazquez, D. J. Milliron, *Nature* **2013**, 500, 323.
- [20] J. Kim, G. K. Ong, Y. Wang, G. Leblanc, T. E. Williams, T. M. Mattox, B. A. Helms, D. J. Milliron, *Nano Lett.* **2015**, 15, 5574.

- [21] Y. Wang, E. L. Runnerstrom, D. J. Milliron, *Annu. Rev. Chem. Biomol. Eng.* **2016**, *7*, 283.
- [22] N. DeForest, A. Shehabi, J. O'Donnell, G. Garcia, J. Greenblatt, E. S. Lee, S. Selkowitz, D. J. Milliron, *Build. Environ.* **2015**, *89*, 107.
- [23] H. K. Pulker, *Coatings on Glass*, Vol. 20, Elsevier, New York **1984**.
- [24] J. Ebisawa, E. Ando, *Curr. Opin. Solid State Mater. Sci.* **1998**, *3*, 386.
- [25] S. D. Rezaei, S. Shannigrahi, S. Ramakrishna, *Sol. Energy Mater. Sol. Cells* **2017**, *159*, 26.
- [26] S. W. Tong, W. P. Goh, X. Huang, C. Jiang, *Renewable Sustainable Energy Rev.* **2021**, *152*, 111615.
- [27] J. Chai, J. Fan, *Mater. Today Energy* **2022**, *24*, 100925.
- [28] P. Pattathil, R. Giannuzzi, M. Manca, *Nano Energy* **2016**, *30*, 242.
- [29] M. Barawi, L. De Trizio, R. Giannuzzi, G. Veramonti, L. Manna, M. Manca, *ACS Nano* **2017**, *11*, 3576.
- [30] S. Zhang, S. Cao, T. Zhang, A. Fisher, J. Y. Lee, *Energy Environ. Sci.* **2018**, *11*, 2884.
- [31] S. Zhang, S. Cao, T. Zhang, Q. Yao, A. Fisher, J. Y. Lee, *Mater. Horiz.* **2018**, *5*, 291.
- [32] S. Cao, S. Zhang, T. Zhang, Q. Yao, J. Y. Lee, *Joule* **2019**, *3*, 1152.
- [33] S. Zhang, S. Cao, T. Zhang, J. Y. Lee, *Adv. Mater.* **2020**, *32*, 2004686.
- [34] Y. Zhai, J. Li, S. Shen, Z. Zhu, S. Mao, X. Xiao, C. Zhu, J. Tang, X. Lu, J. Chen, *Adv. Funct. Mater.* **2022**, *32*, 2109848.
- [35] C. Binet, M. Mitov, M. Mauzac, *J. Appl. Phys.* **2001**, *90*, 1730.
- [36] H. Khandelwal, A. P. H. J. Schenning, M. G. Debije, *Adv. Energy Mater.* **2017**, *7*, 1602209.
- [37] H. Khandelwal, R. C. G. M. Loonen, J. L. M. Hensen, M. G. Debije, A. P. H. J. Schenning, *Sci. Rep.* **2015**, *5*, 11773.
- [38] H. Khandelwal, M. G. Debije, T. J. White, A. P. H. J. Schenning, *J. Mater. Chem. A* **2016**, *4*, 6064.
- [39] W. Hu, H. Zhao, L. Song, Z. Yang, H. Cao, Z. Cheng, Q. Liu, H. Yang, *Adv. Mater.* **2010**, *22*, 468.
- [40] W. Hu, L. Zhang, H. Cao, L. Song, H. Zhao, Z. Yang, Z. Cheng, H. Yang, L. Guo, *Phys. Chem. Chem. Phys.* **2010**, *12*, 2632.
- [41] M. Mitov, M. Mitov, *Adv. Mater.* **2012**, *24*, 6260.
- [42] X. Hu, W. Zeng, W. Yang, L. Xiao, L. T. De Haan, W. Zhao, N. Li, L. Shui, G. Zhou, *Liq. Cryst.* **2019**, *46*, 185.
- [43] G. Cai, A. L. S. Eh, L. Ji, P. S. Lee, *Adv. Sustainable Syst.* **2017**, *1*, 1700074.
- [44] S. Shaik, S. Nundy, V. R. Maduru, A. Ghosh, A. Afzal, *J. Cleaner Prod.* **2022**, *350*, 131444.
- [45] P. M. Chaikin, T. C. Lubensky, T. A. Witten, *Principles of Condensed Matter Physics*, Vol. 10, Cambridge University Press, Cambridge **1995**.
- [46] I. I. Smalyukh, *Annu. Rev. Condens. Matter Phys.* **2018**, *9*, 207.
- [47] H. Mundoor, I. I. Smalyukh, *Small* **2015**, *11*, 5572.
- [48] Q. Zhang, Y. Hu, S. Guo, J. Goebel, Y. Yin, *Nano Lett.* **2010**, *10*, 5037.
- [49] D. H. Sliney, *Eye* **2016**, *30*, 222.
- [50] M. Rycenga, C. M. Cobley, J. Zeng, W. Li, C. H. Moran, Q. Zhang, D. Qin, Y. Xia, *Chem. Rev.* **2011**, *111*, 3669.
- [51] C. Langhammer, B. Kasemo, I. Zorić, *J. Chem. Phys.* **2007**, *126*, 194702.
- [52] D. D. Evanoff, G. Chumanov, *J. Phys. Chem. B* **2004**, *108*, 13957.
- [53] M. Naruse, T. Tani, H. Yasuda, N. Tate, M. Ohtsu, M. Naya, *Sci. Rep.* **2014**, *4*, 6077.
- [54] T. Tani, S. Hakuta, N. Kiyoto, M. Naya, A. Papakostas, A. Potts, D. M. Bagnall, S. L. Prosvirnin, H. J. Coles, *Opt. Express* **2014**, *22*, 9262.
- [55] Y. Matsunami, N. Kiyoto, S. Hakuta, T. Tani, M. Naya, K. Kamada, *Heat Ray-Shielding Material*, U.S. Patent Application No. US20110111210(A1), U.S. Patent and Trademark Office, Washington, DC **2011**.
- [56] G. B. Hadjichristov, Y. G. Marinov, A. G. Petrov, L. Marino, N. Scaramuzza, *J. Phys.: Conf. Ser.* **2016**, *682*, 012015.
- [57] N. Berkovitch, P. Ginzburg, M. Orenstein, *J. Phys.: Condens. Matter* **2012**, *24*, 073202.
- [58] M. Luo, H. Huang, S. Il Choi, C. Zhang, R. R. Da Silva, H. C. Peng, Z. Y. Li, J. Liu, Z. He, Y. Xia, *ACS Nano* **2015**, *9*, 10523.
- [59] G. V. Naik, V. M. Shalaev, A. Boltasseva, *Adv. Mater.* **2013**, *25*, 3264.
- [60] A. V. Ivashchenko, *Dichroic Dyes for Liquid Crystal Displays*, CRC Press, Boca Raton, FL **2018**.
- [61] M. G. Debije, *Adv. Funct. Mater.* **2010**, *20*, 1498.
- [62] T. Burger, C. Sempere, B. Roy-Layinde, A. Lenert, *Joule* **2020**, *4*, 1660.
- [63] I. I. Smalyukh, *Adv. Mater.* **2021**, *33*, 2001228.
- [64] S.-G. Hwang, H.-G. Park, M.-H. Park, S.-G. Park, *J. Vac. Sci. Technol., A* **2018**, *36*, 041401.